

Mechanism and Modeling of Nanorod Formation from Nanodots

Mani Ethayaraja and Rajdip Bandyopadhyaya*[†]

Department of Chemical Engineering, Indian Institute of Technology Kanpur, Kanpur 208016, India

Received January 16, 2007. In Final Form: March 18, 2007

A population balance model based on Smoluchowski aggregation kinetics is developed to explain the formation of nanorods from a colloidal suspension of spherical nanoparticles (nanodots). Our model shows that linear pearl-chain aggregates form by the oriented attachment (OA) of nanodots during the early stages of synthesis, since it occurs with a time scale smaller than the coalescence time scale of nanodots present within an aggregate. The slower coalescence step leads to the transformation of the linear pearl-chain aggregate into a smooth nanorod over a longer time scale of many hours, as observed in experiments. The attachment kinetics is modeled by a modified Brownian collision frequency, with the latter decreasing with nanorod length, leading to the experimentally observed slower growth in nanorod length at longer times. The collision frequency also includes the effects of attractive dipole–dipole and van der Waals interactions between nanodots, which are primarily responsible for OA. Our model predictions are general, and they compare favorably with available experimental data in the literature on the distribution of the aspect ratio (length to diameter) of ZnO and ZnS nanorods over different time scales.

1. Introduction

Anisotropic structures, such as nanorods, have been investigated because of their size- and shape-dependent physical and chemical properties, which can be exploited further for various technical applications. Materials such as nanorods, which are quantum confined in two dimensions, show enhanced properties not accessible in their bulk states.¹ In the quantum confined regime, physical properties can be manipulated by merely changing the size and shape of the nanomaterials. For example, the emission wavelength of a spherical CdSe nanoparticle (quantum confined in all three dimensions) changes from blue to red when its size varies from 1.2 to 11.5 nm.² Nanorods are intensely investigated because their absorption and emission wavelengths are well-separated unlike spherical nanoparticles, called nanodots from hereon. Hence, the reabsorption of emitted light can be eliminated in nanorods.³ Recent reports on nanorod based piezoelectric devices⁴ and solar cells⁵ further motivate us to propose a mechanism of formation of nanorods of controlled diameter and length.

In this paper, we address this issue and develop a model of nanorod formation in a colloidal suspension of nanodots. This can take place when the nanodots are aged in solution under appropriate conditions for a sufficient period of time. This route of nanorod formation offers superior control over both the length and diameter of the nanorods. While the length of the nanorod can be controlled by the aging time, the diameter can be controlled by the preformed nanodot diameter.

So, our work constitutes a crucial step in the overall quest of designing nanorods with specific properties, starting from their synthesis conditions.

Nanorods of different materials, such as ZnO,⁶ ZnS,⁷ Ag,⁸ CdTe,⁹ PbSe,¹⁰ CdSe,¹¹ and so forth, have already been synthesized by the oriented attachment (OA) method. The general problem of aggregation of monomeric units into linear chains is of interest in macromolecules, such as proteins and also inorganic polymers. For example, β -lactoglobulin nanoparticles (~10 nm), a milk serum protein, undergoes irreversible aggregation when heated to 65 °C, causing the protein particles to form linear flexible chains.¹² Similarly, radical addition polymerization (of ethylene, for example) is analogous to these orientation specific aggregation processes, yielding linear chain aggregates.¹³ Aerosol or gas phase routes such as flame synthesis¹⁴ and laser ablation^{14,15} under certain conditions also give rise to linear or branched pearl-chain-like aggregates of individual nanoparticles. These materials can range from metal oxides¹⁴ to elemental carbon.¹⁵ Understanding the mechanism and kinetics of formation of such anisotropic structures is of general interest.

In the context of nanorod formation in solution, it was speculated that the presence of a permanent dipole moment in the nanodots could direct their oriented attachment into a linear chain.^{7,9,10} In the case of quasi-spherical crystalline nanodots, the lack of central symmetry because of the distribution of polar facets may result in dipole moments along the polar faces of nanodots. For ZnO (wurtzite), as an example, 002 faces are polar, because opposite layers are formed by Zn²⁺ and O²⁻, respectively. Similarly, for ZnS (zinc blend), 111 faces are polar, since opposite layers are terminated with Zn²⁺ and S²⁻, respectively. Therefore, the dipole moment arises along the 002 and 111 faces of ZnO

* To whom correspondence should be addressed. Telephone: +91 (22) 2576 7209. Fax: +91 (22) 2572 6895. E-mail: rajdip@che.iitk.ac.in; rajdip@iitk.ac.in.

[†] Present address: Department of Chemical Engineering, Indian Institute of Technology Bombay, Powai, Mumbai 400 076, India.

(1) Rao, C. N. R.; Kulkarni, G. U.; Thomas, P. J.; Edwards, P. P. *Chem.—Eur. J.* **2002**, *8*, 29.

(2) Murray, C. B.; Norris, D. J.; Bawendi, M. G. *J. Am. Chem. Soc.* **1993**, *115*, 8706.

(3) Peng, X.; Manna, L.; Yang, W.; Wickham, J.; Scher, E.; Kadavanich, A.; Alivisatos, A. P. *Nature* **2000**, *404*, 59.

(4) Wang, Z. L.; Song, J. *Science* **2006**, *312*, 242.

(5) Gur, I.; Fromer, N. A.; Geier, M. L.; Alivisatos, A. P. *Science* **2005**, *310*, 462.

(6) Pacholski, C.; Kornowski, A.; Weller, H. *Angew. Chem., Int. Ed.* **2002**, *41*, 1188.

(7) Yu, J. H.; Joo, J.; Park, H. M.; Baik, S.; Kim, Y. W.; Kim, S. C.; Hyeon, T. *J. Am. Chem. Soc.* **2005**, *127*, 5662.

(8) Korgel, B. A.; Fitzmaurice, D. *Adv. Mater.* **1998**, *10*, 661.

(9) Tang, Z.; Kotov, N. A.; Ciersig, M. *Science* **2002**, *297*, 237.

(10) Cho, K. S.; Talapin, D. V.; Gaschler, W.; Murray, C. B. *J. Am. Chem. Soc.* **2005**, *127*, 7140.

(11) Pradhan, N.; Xu, H.; Peng, X. *Nano Lett.* **2006**, *6*, 720.

(12) Roefs, S. P. F. M.; De Kruij, K. G. *Eur. J. Biochem.* **1994**, *226*, 883.

(13) Flory, P. J. *Principles of Polymer Chemistry*; Cornell University Press: New York, 1953.

(14) Bandyopadhyaya, R.; Lall, A. A.; Friedlander, S. K. *Powder Technol.* **2004**, *139*, 193.

(15) Bandyopadhyaya, R.; Rong, W. Z.; Friedlander, S. K. *Chem. Mater.* **2004**, *16*, 3147.

and ZnS nanodots, respectively, resulting in the oriented attachment of nanodots along these faces.^{6,7}

Furthermore, nanodots possess a very high surface area to volume ratio, thus contributing significant surface energy to the total energy of the system. The latter can decrease on nanodot aggregation. However, a stabilizing agent on the nanodot surface prevents aggregation due to steric or electrostatic repulsion, whereas long range dipole interactions between nanodots favor OA. When the latter factor predominates the former, for example, on partial removal of the stabilizing agent, spontaneous OA of nanodots occurs. The very specific ordering of dots into linear chains is mainly because of directional dipole moments, arising due to opposite polarity of the crystal planes. Thus, rods form mostly in the direction of the dipole moment, and no side branching occurs. In fact, most of the experiments on OA report nanorods as the only structure formed.^{6–9,11} Our model, being based on systems with unidirectional orientation, also aims to describe nanorod formation. However, in one study, Cho et al.¹⁰ optimized experimental conditions to engineer the direction of the dipole moment, thereby manipulating aggregation along faces other than the polar faces, resulting in branched nanostructures (rectangular rings, star-shapes, and so forth), which is beyond the scope of the present model.

To address the kinetics of formation of long one dimensional nanostructures starting from primary monomeric particles (nanodots in our case), a general mechanism based on experimental facts should be formulated. We conceive it to consist of two processes: (i) oriented attachment of a preformed suspension of nanodots, whereby the dots aggregate to form linear pearl-chain structures and (ii) coalescence of preformed nanodots within the chain aggregate. The two steps can take place simultaneously, or they may be separated in time if their time scales are different. Our focus is to derive a general model which should predict the length to diameter aspect ratio of nanorods measured under different experimental conditions and be applicable for different materials.

2. Population Balance Model

Previously, Huang et al.¹⁶ considered dimer formation by Brownian collision of nanodots and dimer growth by Ostwald ripening to predict the temporal evolution of the average size of ZnS nanoaggregates (not necessarily nanorods) under hydrothermal conditions. Since they did not consider structures larger than a dimer, their model does not apply to the formation of nanorods with a reasonably large aspect ratio. Later, Sinyagin et al.,¹⁷ from Monte Carlo simulations, found that an increase in the nanodot dipole moment produced longer chain aggregates rather than other nonlinear or branched structures. In the absence of a dipole moment, otherwise, random Brownian collision of nanodots results in only branched fractal aggregates.

We now develop a set of equations that describe the process of collision and the OA of nanodots into linear chain aggregates. It is of relevance to mention that we had previously modeled nanodot formation and predicted individual nanodot size^{18–22} using the population balance equation (PBE). In the present work,

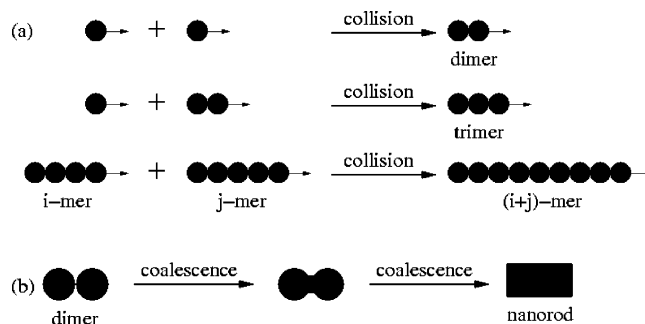


Figure 1. Sequential steps in the mechanism of the formation of nanorods from nanodots. (a) Linear pearl-chain formation by oriented attachment (OA) of nanodots. Arrows in the nanodots and linear chains show the representative direction of the dipole moment. (b) Coalescence of nanodots in a dimer (a representative linear chain) to form smooth nanorods.

we utilize the PBE framework to describe the assembly of such individual dots into larger structures such as rods.

Let N_0 be the initial (at time $t = 0$) number density of nanodots present in the aging solution. These nanodots undergo Brownian collision because of their very small size of a few nanometers. In such collisions, nanodots aggregate to form dimers, trimers, and so forth, which further aggregate to form highly oriented linear chains as shown in Figure 1a. Collisions between linear chain aggregates occur such that they attach only at their two ends.

In the absence of any interaction potential between the aggregates, the Brownian collision frequency of two linear chain aggregates containing i and j numbers of nanodots, respectively, is given by²³

$$q(i,j) = 4\pi(D_i + D_j)(R_i + R_j) \quad (1)$$

where D_i and D_j are the diffusion coefficients of the chain aggregates. The radii of the linear chain aggregates R_i and R_j are given by iR_p and jR_p , respectively, where R_p is the radius of a nanodot. The diffusion coefficient of the aggregates is calculated from the Stokes–Einstein equation as follows.

$$D_i = \frac{k_B T}{6\pi\mu R_i} \quad (2)$$

Substituting D_i and D_j in eq 1, we get

$$q(i,j) = \frac{2k_B T}{3\mu} \left(2 + \frac{i}{j} + \frac{j}{i} \right) \quad (3)$$

Aggregation is described by the Smoluchowski aggregation model as follows.²³

$$\frac{dn_k}{dt} = \frac{1}{2} \sum_{i=1}^{k-1} q(k-i, i) n_{k-i} n_i - n_k \sum_{i=1}^{\infty} q(i, k) n_i \quad (4)$$

In this equation, the first term on the right-hand side represents the rate at which the population of chain aggregates (n_k) is formed due to aggregation of smaller, appropriately sized aggregates. The factor $1/2$ is required because of double counting in the summation. The second term is the rate of disappearance of n_k due to aggregation with any other aggregate or nanodot. According to this model given by eq 4, no specific orientation of nanodots takes place, rather it results in a disordered fractal aggregate.

(23) Friedlander, S. K. *Smoke, Dust, and Haze: Fundamentals of Aerosol Dynamics*; Oxford University Press: New York, 2000.

(16) Huang, F.; Zhang, H.; Banfield, J. F. *Nano Lett.* **2003**, *3*, 373.

(17) Sinyagin, A.; Belov, A.; Kotov, N. A. *Modelling Simul. Mater. Sci. Eng.* **2005**, *13*, 389.

(18) Bandyopadhyaya, R.; Kumar, R.; Gandhi, K. S. *Langmuir* **2001**, *17*, 1015.

(19) Ethayaraja, M.; Dutta, K.; Bandyopadhyaya, R. *J. Phys. Chem. B* **2006**, *110*, 16471.

(20) Ethayaraja, M.; Bandyopadhyaya, R. *J. Am. Chem. Soc.* **2006**, *128*, 17102.

(21) Ethayaraja, M.; Ravikumar, C.; Muthukumar, D.; Dutta, K.; Bandyopadhyaya, R. *J. Phys. Chem. C* **2007**, *111*, 3246.

(22) Ethayaraja, M.; Dutta, K.; Muthukumar, D.; Bandyopadhyaya, R. *Langmuir* **2007**, *23*, 3418.

However, for the mechanism under study (the oriented attachment of nanodots into linear chains), aggregation is highly orientation specific. So, a nanodot or a chain attaches only at one particular end of another growing linear chain aggregate (Figure 1a). To include this correction in eq 3, a probability function that depends on the chain length of the colliding aggregate is introduced.

Consider two linear chains consisting of i and j nanodots, respectively (Figure 1a). Since the dipole moment arises due to the opposite polarity of the two faces (top and bottom), OA is possible only if the top (or bottom) face of the first (last) nanodot in one chain collides with the bottom (or top) face of the last (first) nanodot in another. Each nanodot is analogous to a magnet, and hence the number of successful collisions leading to OA is only two out of a total of ij possible attachment positions. Therefore, the probability of OA by attachment at the chain ends is given by $2/(ij)$.

The inclusion of interaction potentials due to dipole–dipole and van der Waals interactions is another modification in the Brownian collision frequency that is done in the present model. The frequency then becomes $q(i,j)/W$ on including an interaction potential (ϕ) among the colliding aggregates. The correction factor W is related to ϕ for equal sized nanodots as²³

$$W = 2R_p \int_{2R_p}^{\infty} \frac{\exp(\phi/k_B T)}{h^2} dh \quad (5)$$

Here, h is the center to center separation distance of the nanodots. ϕ is given by

$$\phi = - \frac{p^2}{2\pi\epsilon_0 h(h^2 - 4R_p^2)} - \frac{A_H}{6} \left[\frac{2R_p^2}{h^2 - 4R_p^2} + \frac{2R_p^2}{h^2} + \ln \left(\frac{h^2 - 4R_p^2}{h^2} \right) \right] \quad (6)$$

The first term on the right-hand side of eq 6 is for the attractive interaction potential due to aligned dipole–dipole attraction. The second term denotes van der Waals attractive interactions. A_H is the Hamaker constant of the nanodots, and p is the dipole moment. As ϕ is negative, W is less than one, and hence the collision frequency will be increased due to these interactions. The W value calculated from eqs 5 and 6 is used here for the collision of linear chains.

Therefore, the modified form of the Brownian collision frequency after including the two modifications discussed above is given by

$$\bar{q}(i,j) = \frac{q(i,j)}{W} \left(\frac{2}{ij} \right) = \frac{2k_B T}{3\mu W} \left(2 + \frac{i}{j} + \frac{j}{i} \right) \left(\frac{2}{ij} \right) \quad (7)$$

Equation 4 then becomes

$$\frac{dn_k}{dt} = \frac{1}{2W} \sum_{i=1}^{k-1} q(k-i,i) \left[\frac{2}{(k-i)i} \right] n_{k-i} n_i - \frac{1}{W} n_k \sum_{i=1}^{\infty} q(i,k) \left(\frac{2}{ik} \right) n_i \quad (8)$$

Substituting eq 3 into eq 8 and scaling n_k by N_0 , we get

$$\frac{d\bar{n}_k}{dt} = \frac{1}{2\tau_c} \sum_{i=1}^{k-1} \left(2 + \frac{k-i}{i} + \frac{i}{k-i} \right) \left[\frac{2}{(k-i)i} \right] \bar{n}_{k-i} \bar{n}_i - \frac{1}{\tau_c} \bar{n}_k \sum_{i=1}^{\infty} \left(2 + \frac{i}{k} + \frac{k}{i} \right) \left(\frac{2}{ik} \right) \bar{n}_i \quad (9)$$

Table 1. Parameters Used in the Present Model

parameter	value	ref
A_H for ZnO	8.69×10^{-21} J	calculated from the Lifshitz theory ²⁵
A_H for ZnS	4.85×10^{-20} J	calculated from the Lifshitz theory ²⁵
N_0	10^{24} m ⁻³	estimated from 6
p	50 D	9
R_p for ZnO	1.5 nm	6
R_p for ZnS	2.5 nm	7
T	333 K	6,7
v_{mol} for ZnO	2.41×10^{-29} m ³ /molecule	calculated
v_{mol} for ZnS	3.95×10^{-29} m ³ /molecule	calculated
β for ZnO	5.52×10^{-11}	fitted ^a
β for ZnS	1.89×10^{-11}	fitted ^a
ϵ (for methanol)	30	26
γ	0.1 J m ⁻²	18
μ	0.001 kg m ⁻¹ s ⁻¹	standard value

^a Corroborates with the range of values of Huang et al.¹⁶

where, $\bar{n}_k = n_k/N_0$, $\tau_c = (\beta q_0 N_0/W)^{-1}$, and $q_0 = 2k_B T/3\mu$. β is the efficiency of collision and OA, indicating the fraction of collisions leading to the actual attachment of solid nanodots. Therefore, dependence on the nanodot material and different experimental conditions influencing Brownian collision and OA can be lumped together in β .

Finally, eq 9 is solved to obtain the length distribution of linear chains as a function of time with the following initial conditions.

$$\begin{aligned} \bar{n}_k(t=0) &= 1 & \text{for } k=1 \\ &= 0 & \text{for } k>1 \end{aligned} \quad (10)$$

In solving eq 9, we need W . The latter is independent of time, and hence it can be calculated separately from eqs 5 and 6. The parameter values used in solving eq 9 together with eqs 5 and 6 are given in Table 1.

Nanodots coalesce with neighboring nanodots within the same aggregate chain to gradually transform into smooth nanorods, as shown schematically in Figure 1b. The figure shows the intermediate stage of coalescence by solid-state diffusion of molecules between neighboring nanodots. The final nanorod has a smooth surface topography, without any trace of the underlying aggregate structure of the initial, individual spherical dots. Experimentally, it was observed that the diameter of nanorods was same as that of the nanodots, which is in conformity with the mechanism in Figure 1.^{6,7,9,10} The kinetics of coalescence of two solid particles undergoing solid-state diffusion is given by²³

$$\frac{da_i}{dt} = - \frac{1}{\tau} (a_i - a_{m,i}) \quad (11)$$

In this equation, a_i is the actual surface area of the aggregate at any stage of coalescence, containing i nanodots, whereas $a_{m,i}$ is the minimum surface area of the aggregate corresponding to a cylindrical rod. τ is the time constant of coalescence, which is defined as

$$\tau = \frac{3}{64\pi} \frac{k_B T v_p}{\gamma D v_{mol}} \quad (12)$$

Here, v_p is the volume of a nanodot, D is the solid-state diffusion coefficient, γ is the surface free energy, and v_{mol} is the volume of one molecule of the nanodot material.

D depends on temperature according to the Arrhenius form as

$$D = D_0 \exp\left(-\frac{E}{RT}\right) \quad (13)$$

where D_0 is the pre-exponential factor and E is the activation energy of diffusion.

As the process of coalescence strictly conserves the aggregate volume, and nominally the nanodot diameter, eq 11 becomes

$$\frac{dL_i}{dt} = -\frac{1}{\tau}(L_i - L_{m,i}) \quad (14)$$

where L_i is the length of the linear chain aggregate. In our model, the length of a nanorod (L_i), having i nanodots, is obtained by multiplying the number of primary nanodots (i) with the diameter of the nanodot ($2R_p$). $L_{m,i}$ in eq 14 is then given by $4iR_p/3$.

Integrating eq 14, we get

$$\frac{L_i(t) - L_{m,i}}{L_i(t=0) - L_{m,i}} = \exp\left(-\frac{t}{\tau}\right) \quad (15)$$

where $L_i(t=0) = 2iR_p$. Using eq 15, we can estimate the time required for a given extent of coalescence. Let X be the fractional extent of coalescence, which refers to the extent of fusion-mediated smoothening of the curved region, formed at the contact point of two nanodots (when two dots form an aggregate). It is a measure of the fractional extent to which a linear chain aggregate has transformed into a smooth cylindrical nanorod.

Substituting for $L_{m,i}$ and L_i in eq 15, we get

$$t = -\tau \ln\left[\frac{2(1-X)}{X}\right] \quad (16)$$

We have taken X to be 0.99 to consider a structure as a smooth nanorod, which therefore will have almost no identifiable discrete particulate structure at the surface, as shown in Figure 1. The calculated time (τ_{cs}) for $X = 0.99$ from eq 16 is $\sim 4\tau$. This value ($\tau_{cs} = 4\tau$) is used as the time scale of coalescence and smoothening in further discussion.

3. Results and Discussion

The present model is capable of predicting the distribution of the aspect ratio (AR = length to diameter ratio) of nanorods formed by OA of corresponding nanodots. Experimental data on AR distribution of ZnO and ZnS nanorods,^{6,7} synthesized under different experimental conditions, have been used to compare predictions from the present model. ZnO nanorods were formed by OA of preformed quasi-spherical ZnO nanodots (mean size = 3 nm), when a methanolic solution of nanodots was refluxed continuously for 2 h at 60 °C.⁶ Transmission electron microscopic (TEM) images at 2 h showed a mixture of individual nanodots along with some aggregated nanodots forming linear pearl-chain-like structures. After 24 h of aging, the images showed that almost all the nanodots were converted into smooth ZnO nanorods. In another experiment, zinc blend (cubic) structured ZnS nanorods were formed by OA of hexadecylamine (surfactant) coated ZnS nanodots (mean size = 5 nm), when the latter were aged in oleylamine at 60 °C.⁷ In an observation made after 1 h of aging, the authors obtained a mixture of nanodots and linear aggregates in the TEM images. On further aging for 24 h, the images showed the presence of partially smoothened nanorods. In both these experiments, the diameter of the nanorods formed by aging was same as that of the starting nanodot. This observation further

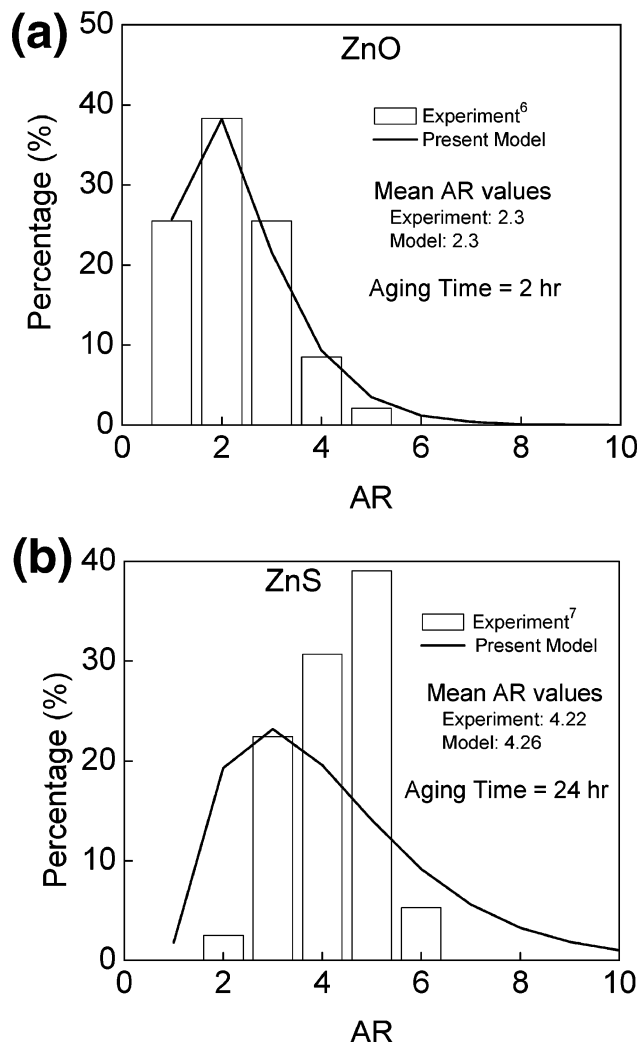


Figure 2. Comparison of experimental and model predictions of the length to diameter aspect ratio (AR) distribution of nanorods of (a) ZnO and (b) ZnS.

substantiates that OA of nanodots along a preferred axis is the beginning step of nanorod formation. The underlying mechanism of nanorod formation in these different systems can be common, which is tested against the present model.

In both ZnO and ZnS nanorod formation, the model results match very closely with the experimental mean AR values as listed in Figure 2. In addition, the model also predicts the experimental AR distribution fairly well. While for ZnO the comparison is nearly exact (Figure 2a), the prediction deviates to some extent from the experimental AR distribution for ZnS. The shape of the predicted distribution depends on a correct estimate of the diffusion coefficient of linear aggregates (D_i). In our model, we calculated D_i using the Stokes–Einstein equation (eq 2). However, according to the definition of eq 2, D_i is the diffusion coefficient of an impermeable sphere with a radius R_i ($= iR_p$). Therefore, it is possible that, on using eq 2, we overestimate D_i of linear aggregates, which results in a broader distribution of the AR of nanorods (Figure 2b). However, the deviation in the distribution of the AR between the model and experiment is very small for ZnO nanorods (Figure 2a) because the simulation results are shown at 2 h, within which time only small nanorods form. Therefore, the approximation of using the Stokes–Einstein equation for small aggregates may be acceptable, but not when the aggregates become relatively longer at 24 h.

One of the characteristic features of our model is the detailed accounting of the collision rate, consisting of the Brownian

Table 2. Comparison of the Time Scales of Collision and Coalescence of Nanodots and the Corresponding Experimental Aging Times

material	time scale of collision and OA, τ_c (h)	time scale of coalescence and smoothening, $\tau_{cs} = 4\tau$ (h) ^a	aging times used in experiments, τ_a (h) ^{6,7}		time scale comparison	
			observation 1	observation 2	for observation 1	for observation 2
ZnO	3.3	13.3	2	24	$\tau_a < \tau_c < \tau_{cs}$	$\tau_c < \tau_{cs} < \tau_a$
ZnS	7.1	38.9	1	24	$\tau_a < \tau_c < \tau_{cs}$	$\tau_c < \tau_a < \tau_{cs}$

^a D is calculated from eq 13 using the typical values for activation energy ($E = 100$ kJ/mol), pre-exponential factor ($D_0 = 10^{-5}$ m² s⁻¹), and $T = 298$ K.

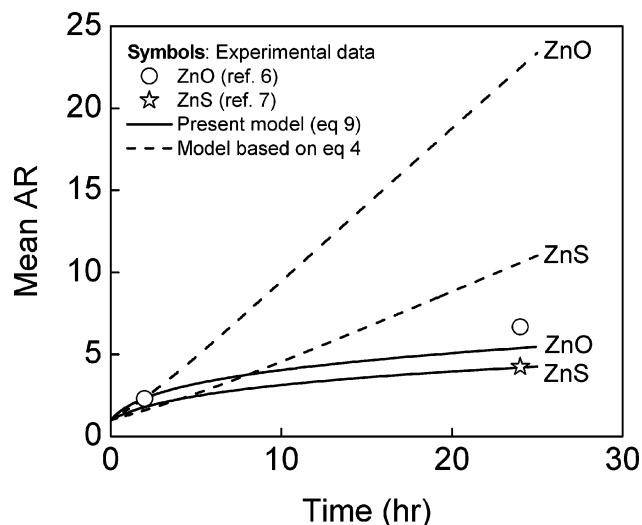


Figure 3. Comparison between experiments and model predictions of the temporal evolution of the mean values of the ZnO and ZnS nanorod aspect ratio (AR) using the classical Brownian collision frequency (eq 4) and the present model (eq 9).

collision frequency, the effect of attractive interaction (W), the attachment probability factor ($2/ij$), and the collision efficiency (β). Since all other factors except β can be theoretically calculated, we fitted β to match the experimental results. The fitted β values are within the range of values reported in the literature. For example, Huang et al.¹⁶ reported lumped OA rates (kN_0 , which is equivalent to $\beta q_0 N_0 / W$ in our model) for ZnS nanodots in the range of 0.07–63.4 h⁻¹. Hence, our $\beta q_0 N_0 / W$ values for ZnS and ZnO nanorods correspond to kN_0 values of 0.14 and 0.30 h⁻¹, respectively, and are therefore within the reported range.

The agreement between the model and experimental results for two different systems shows the generality of the PBE model. Experiments also showed that, in the early stages of aging, linear chain aggregates were formed, but on continued aging, they transformed to smooth nanorods.^{6,7,9,10} We give a qualitative explanation of this fact based on the comparison of time scales from our model.

Table 2 shows the collision and coalescence time scales of nanodots and compares them with experimental data at different aging times. In ZnO nanorod formation, the time scale of collision and OA of nanodots into linear chain aggregates (3.3 h) is smaller compared to the coalescence time of nanodots (13.3 h). This implies that nanodots attach to each other to form chain-like aggregates by Brownian collision at a rate faster than that of the coalescence of two nanodots. Therefore, in the observation at 2 h (observation 1 for ZnO in Table 2), which is less than the collision time, one expectedly sees a mixture of nanodots and linear aggregates in experiment (Figure 3a in ref 6). This is because the 2 h time period is less compared to the collision time (3.3 h), giving a mixture of dots and aggregates. Further, the 2 h observation time is also much shorter compared to the time scale of coalescence and smoothening (13.3 h), preventing the

complete transformation of linear aggregates into smooth nanorods. However, the authors reported that almost all the nanodots were converted into smooth ZnO nanorods after 24 h of aging (observation 2 for ZnO in Table 2).⁶ This also is expected, as the aging time of 24 h is higher than the coalescence time. To summarize, given that $\tau_c < \tau_{cs}$, (i) linear chain aggregates would be observed if $\tau_a < \tau_c$ and (ii) smooth nanorods would be observed if $\tau_a > \tau_{cs}$.

The above explanation also applies for ZnS nanostructures. The time scale of collision and OA of ZnS nanodots (7.1 h) is smaller compared to their coalescence time scale (38.9 h). Therefore, after aging for 1 h (observation 1 for ZnS in Table 2), which is even less than the collision time scale (7.1 h), the authors expectedly obtained a mixture of nanodots and linear aggregates. Further aging of up to 24 h (observation 2 for ZnS in Table 2), which is in between the collision and coalescence time limits, suggests that there will be no nanodots left in the system; rather linear chain aggregates that are only partially transformed into nanorods will be seen. Indeed, the TEM images (Figure 1b in ref 7) did show ZnS nanorods with a rough surface topology, an indication of partial smoothening of linear chain aggregates, as an intermediate stage toward smooth ZnS nanorod formation.

The general transition mechanism from linear chain aggregate to smooth nanorods is also seen in the formation of CdTe nanorods.⁹ For example, after aging CdTe nanodots for 2 days (48 h) at room temperature, chain aggregates were formed. Further aging up to 7 days (168 h) gave nanorods. The longer amount of time (of the order of 2–7 days) taken for the formation of CdTe nanorods, compared to ZnS nanorod formation, is probably due to the much slower coalescence rate of CdTe, due to its lower diffusion coefficient.²⁴

We also found that, for calculating end-to-end collision of nanorods, inclusion of the probability factor ($2/ij$) in eq 7 is vitally important. As shown in Figure 3, if the classical Brownian collision frequency is used, the mean AR value of nanorods constantly increases with time. Furthermore, AR distribution becomes broader with time in this case, because longer chains increase in length at a faster rate than the shorter chains (eq 3). Contrary to this, reasonably narrow AR distributions of nanorods are often observed in experiments.^{6,7} This in turn implies that, in general, longer nanorods have a smaller probability to undergo OA with other nanorods, as shown previously by eq 7.

In Figure 3, the model results from both these possibilities (classical Brownian collision frequency and the present model) are shown. The mean AR values of ZnO predicted from the present model are close to the experimental values at 2 and 24

(24) Shaw, D. J. *Phys. C: Solid State Phys.* **1984**, *17*, 4759.

(25) Hunter, R. J. *Foundations of Colloid Science*; Oxford University Press: New York, 1987; Vol. 1.

(26) Lide, D. R. *CRC Handbook of Chemistry and Physics*; CRC Press: Boca Raton, FL, 2004.

h of aging. On the other hand, classical Brownian collision based results show a constant increase of the mean AR, which overestimates the experimental data very significantly. A similar conclusion can be reached (Figure 3) for the case of ZnS nanorods as well, although there is only one available data point (mean AR) at 24 h. Therefore, independent of the material details, the evolution of the mean AR is well within the range of our model prediction, whereas classical Brownian collision results are significantly different and have no predictive value. Hence, our model is general and is capable of giving a reasonably correct AR value of evolving nanostructures, without going into specific details of the nature and facets of crystalline forms of ZnO, ZnS, or other oriented dipoles. From the foregoing discussion, it is clear that the present model captures the underlying mechanism of OA of nanodots and their slow transformation to nanorods by coalescence and smoothing.

4. Conclusion

The formation of nanorods by oriented attachment (OA) and coalescence of nanodots is proposed as a new mechanism. This mechanism is translated into a population balance equation, with a modified Brownian collision frequency of nanodots. We account for attractive interactions (due to dipole–dipole and van der Waals interactions) between the dots, which lead to the experimentally observed pearl-chain-like aggregates of dots by the OA mechanism. The modification of Brownian collision in our model captures the dependence of nanorod growth on nanorod length, resulting in a decrease of collision frequency with an increase in chain length. Thus, our model results match the experimentally measured distribution of the length to diameter aspect ratio (AR) of ZnO and ZnS nanorods reasonably well.

A time-scale comparison between the two competing processes of (i) OA of nanodots using modified Brownian collision and (ii) coalescence of nanodots within an aggregate shows that the former is faster compared to the latter. Hence, linear pearl-chain aggregates form during the early stages of nanodot aging. However, when sufficient aging time (equal to or more than the coalescence time scale of the nanodots) is provided, linear chain aggregates transform into smooth nanorods. These findings are corroborated with experimental data. Chain aggregates of ZnO were seen after only 2 h of aging ($\tau_a < \tau_c$), which transformed into smooth ZnO nanorods after aging for 24 h ($\tau_a > \tau_{cs}$).⁶ Similarly, a mixture of nanodots and short linear aggregates of ZnS formed after 1 h of aging ($\tau_a < \tau_c$), while linear chain aggregates partially transformed into ZnS nanorods ($\tau_c < \tau_a < \tau_{cs}$) after 24 h of aging. Similar arguments are extended for CdTe nanorod formation as well.

While the classical Brownian collision frequency fails to explain the temporal evolution of the mean AR of nanorods, the present model very successfully captures this trend, across different materials and experimental conditions, lending some generality in our mechanism and proposed model calculations. Analyses of the model results can therefore provide us with a way to control the length and surface topography of nanorods (smooth cylindrical nanorod versus particulate chain aggregate of spherical nanodots) by suitably tuning the relative rates of collision and coalescence. The latter, for example, can be achieved by changing the solvent, additives, aging time, and so forth. The diameter of the nanorod, on the other hand, can be controlled by the diameter of the preformed nanodots. These findings will therefore open up further investigation in the relatively new and emerging areas of synthesis, structure, and dynamics of anisotropic nanostructures.

Specific ordering of nanodots into linear chains (and hence into nanorods) in experiments takes place because of the directional dipole moment, with the latter arising due to the opposite polarity of the crystal planes in the nanodots. The nanorod is thus the dominant product in most experiments, the kinetics of which process we model by combining OA and coalescence. The mechanism and precise experimental conditions of the formation of other anisotropic structures, such as nanorings and so forth, are not clearly known and are therefore outside the scope of the present model.

Glossary

a_i	Surface area of an aggregate consisting of i number of nanodots, m^2
$a_{m,i}$	Minimum surface area of an aggregate consisting of i number of nanodots, m^2
A_H	Hamaker constant of nanodots, J
D	Diffusivity of nanodots (eq 13), $m^2 s^{-1}$
D_0	Pre-exponential factor in eq 13, $m^2 s^{-1}$
D_i	Diffusivity of linear chain aggregates containing i number of nanodots, $m^2 s^{-1}$
E	Activation energy of diffusion, $kJ mol^{-1}$
h	Center to center separation distance of nanodots, m
i	Subscript, used to denote the number of nanodots in a linear chain aggregate
k	Rate constant of collision of nanodots (defined in eq 6 of ref 16), $m^3 s^{-1}$
k_B	Boltzmann constant, $1.3806 \times 10^{-23} J K^{-1}$
$L_i(t)$	Length of an aggregate consisting of i number of nanodots at time t , m
$L_{m,i}$	Minimum length of an aggregate consisting of i number of nanodots, m
N_0	Initial (at time, $t = 0$) number density of nanodots, m^{-3}
n_k	Number density of aggregates containing k number of nanodots, m^{-3}
\bar{n}_k	Nondimensional number density of aggregates containing k number of nanodots
p	Dipole moment of nanodots, Debye
q	Collision frequency of aggregates, $m^3 s^{-1}$
q_0	Prefactor in eq 3, defined as $q_0 = 2k_B T/3\mu$
R	Ideal gas constant, $8.314 J mol^{-1} K^{-1}$
R_i	Radius of a linear chain aggregate consisting of i number of nanodots, m
R_p	Radius of a single nanodot, m
t	Time, s
T	Temperature, K
v_p	Volume of a nanodot, m^3
v_{mol}	Volume of a ZnO or ZnS molecule, m^3
W	Correction factor in collision frequency due to inter-nanodot interactions
X	Fractional extent of coalescence of linear chain aggregates
β	Collision and oriented attachment efficiency of nanodots
ϵ	Permittivity of the aging solution
ϵ_0	Permittivity of vacuum, $8.854 \times 10^{-12} C^2 J^{-1} m^{-1}$
γ	Surface free energy of nanodots, $J m^{-2}$
μ	Viscosity of the aging solution, $kg m^{-1} s^{-1}$
ϕ	Interaction potential among the colliding aggregates, J
τ	Time constant of coalescence, s
τ_a	Experimental aging time, s
τ_c	Time scale of collision and oriented attachment of nanodot aggregates, s
τ_{cs}	Time scale of coalescence and smoothing of nanodot aggregates to nanorods, s